

New Preparation Method of Gold Nanoparticles on SiO₂

Rodolfo Zanella,^{*,†,‡} Alberto Sandoval,[†] Patricia Santiago,[§] Vladimir A. Basiuk,^{⊥,‡} and José M. Saniger^{†,‡}

Centro de Ciencias Aplicadas y Desarrollo Tecnológico, Universidad Nacional Autónoma de México (UNAM), Circuito Exterior S/N, A. P. 70-186, C. P. 04510, Ciudad Universitaria, México D. F., Mexico, Instituto de Física, UNAM, Circuito de la Investigación Científica S/N, C. P. 04510, Ciudad Universitaria, México D. F., Mexico, and Instituto de Ciencias Nucleares, UNAM, Circuito Exterior, A. P. 70-543, C. P. 04510, Ciudad Universitaria, México D. F., Mexico

Received: January 27, 2006; In Final Form: March 9, 2006

It is shown that adsorption of the [Au(en)₂]³⁺ cationic complex can be successfully employed for the deposition of gold nanoparticles (1.5 to 3 nm) onto SiO₂ with high metal loading, good dispersion, and small Au particle size. When the solution pH increases (from 3.8 to 10.5), the Au loading in the Au/SiO₂ samples increases proportionally (from 0.2 to 5.5 wt %), and the average gold particle size also increases (from 1.5 to 2.4 nm). These effects are explained by the increase in the amount of negatively charged sites present on the SiO₂ surface, namely, when the solution pH increases, a higher number of [Au(en)₂]³⁺ species can be adsorbed. Extending the adsorption time from 2 to 16 h gives rise to an increase in the gold loading from 3.3 to 4.0 wt % and in the average particle size from 1.8 to 2.9 nm. Different morphologies of gold nanoparticles are present as a function of the particle size. Particles with a size of 3–5 nm show defective structure, some of them having a multiple twinning particle (MTP) structure. At the same time, nanoparticles with an average size of ca. 2 nm exhibit defect-free structure with well-distinguishable {111} family planes. TEM and HAADF observations revealed that Au particles do not agglomerate on the SiO₂ support: gold is present on the surface of SiO₂ only as small particles. Density functional theory calculations were employed to study the mechanisms of [Au(en)₂]³⁺ adsorption, where neutral and negatively charged silica surfaces were simulated by neutral cluster Si₄O₁₀H₄ and negatively charged cluster Si₄O₁₀H₃, respectively. The calculation results are totally consistent with the suggestion that the deposition of gold takes place according to a cationic adsorption mechanism.

Introduction

At the end of the 80's an exceptionally high catalytic activity of gold nanoparticles supported on metal oxides was discovered for the CO oxidation,^{1–6} which was interpreted as the formation of an active Au/support interface along the perimeter of gold particles.^{7,8} The Au/support interface is a model of a metal–semiconductor or metal–insulator junction bearing unique size-dependent electronic properties, which could play an essential role in the origin of the high catalytic activity.

Following this assumption, the specific support materials should play an important role in the catalytic behavior of gold. The supports, generally being metal oxides, are divided into two categories: the reducible (Fe₂O₃, TiO₂, Co₂O₃, CeO₂, ZrO₂) and the nonreducible supports (SiO₂, Al₂O₃, MgO).⁸ The nature of the active species is still being discussed. It has been suggested that the role of the metal oxide support is the stabilization of the gold nanoparticles, and that the CO oxidation takes place on the gold surface.^{9–15} Other authors have proposed that the reaction takes place at the gold/metal oxide interface, and that the metal oxide support could act as a source of

oxygen.^{6,8,16–21} To elucidate this question, the electronic structure and catalytic activity of Au nanoparticles has to be characterized in the absence of any supporting material; however, this is technically difficult. In our opinion, an alternative approach for an experimental study of this subject is the deposition of Au nanoparticles onto a noncatalytic, inactive substrate. Silica satisfies these requirements well.

Silica is used as a support because of its inert character, which allows investigation of the effect of the metal, minimizing the effect of the metal–support interaction. The weak interaction between SiO₂ surfaces and Au particles makes silica supports very convenient for studying the size effect of the gold nanoparticles on their catalytic activity, minimizing the disturbance of the support interaction.²²

Gold catalysts on an inert oxide support, such as SiO₂, need to be prepared in a highly dispersed state. Indeed, for these systems, oxygen activation is not expected to occur on the support, but on the gold particle surface.⁸ An enhanced activity may also arise from geometric effects associated with defect sites such as kinks, steps, and edges, or from electronic effects arising from variations in the density of states of small gold particles.^{15,23,24}

Liquid-phase preparation methods such as deposition–precipitation, coprecipitation, and impregnation have not been effective in supporting small gold particles on SiO₂.^{6,25–27} The difficulty of depositing highly dispersed gold nanoparticles on SiO₂ by liquid-phase methods arises from the fact that the point

* Address correspondence to this author. E-mail: zanella@aleph.cinstrum.unam.mx. Phone: +(52) 555-622-8602, ext. 1115. Fax: +(52) 555-622-8651.

† Centro de Ciencias Aplicadas y Desarrollo Tecnológico.

‡ Members of UNAM Nanotechnology Project (PUNTA).

§ Instituto de Física.

⊥ Instituto de Ciencias Nucleares.

of zero charge (PZC) for SiO₂ surfaces is close to pH 2. This fact means that the SiO₂ surface becomes negatively charged above pH 2, complicating the deposition of anionic gold species such as (AuCl₄)⁻. For this reason, when these methods are applied to deposit gold on SiO₂, the average nanoparticle diameter becomes very large (20 nm),²⁵ and no detectable catalytic activity for CO oxidation at low temperature is observed.²⁶

Many attempts have been undertaken to obtain small gold particles on SiO₂ by using different experimental approaches. Gold particles of 10–50 nm diameter on SiO₂/Si(100) were created by Ar⁺ ion implantation of a bulklike Au/SiO₂/Si(100) thin film.²² A strategy to immobilize gold nanoparticles (5 nm) on SiO₂ surfaces has been developed by embedding the gold particles into a layer of octadecylsiloxane or into multiple layers of SiO₂ created by deposition and oxidation of octadecylsiloxane self-assembled monolayers.²⁸ Okumura et al.²⁹ prepared gold particles (6.6 nm) on SiO₂ by chemical vapor deposition (CVD), which showed a high catalytic activity in the CO oxidation. Au/SiO₂ prepared by the CVD method exhibits catalytic activity for CO oxidation as high as Au/Al₂O₃ and Au/TiO₂ do. This could indicate that the reason for the low catalytic activity, usually found for the Au/SiO₂ systems, cannot be simply attributed to the nature of the support, but that the procedure of preparation is also crucial. Au/SiO₂ has also been prepared by CVD of dimethylgold(III) β -diketone,³⁰ but the problem of CVD methods is that the volatile Au precursors used are very expensive.

Taking into account the fact that SiO₂ is an amphoteric oxide (isoelectric point IEP_{SiO₂} = 2),³¹ this oxide can be used for the adsorption of cationic metallic species when the solution pH is higher than IEP_{SiO₂}. Iler³² has proposed a mechanism of silica dissolution in basic medium, which involves OH⁻ ions as catalysts of silica depolymerization; indeed, for pH lower than 11, the Si(OH)₅⁻ species released is hydrolyzed into silicic acid Si(OH)₄, and the OH⁻ ions are regenerated.

In basic medium, Si(OH)₄ units can condense, be ionized [SiO(OH)₃]⁻, and form different types of monomeric, oligomeric, and negatively charged polymeric chains.

In the case of gold, [Au(en)₂]³⁺ complex (en = ethanediamine), whose synthesis was described by Block and Bailar,³³ has been successfully used by Guillemot et al.^{34,35} for the introduction of gold into Y zeolites by cationic exchange and by one of us to deposit Au/TiO₂^{25,36} by cationic adsorption. Until now (to the best of our knowledge) nobody has tried the adsorption of cationic [Au(en)₂]³⁺ complex on SiO₂.

The goal of this study is therefore to investigate whether it is possible to prepare Au/SiO₂ catalysts with small metal particles based on the adsorption of cationic [Au(en)₂]³⁺ complex, in the same size range as for the samples prepared on TiO₂ by the same method.^{25,36} In this way, a new and simple liquid-phase method for the preparation of Au/SiO₂ would be available, allowing for a more reliable comparison of the activities of gold nanoparticles supported on reducible and inert supports, both prepared by the same experimental approach.

In this paper, we show for the first time that adsorption of cationic [Au(en)₂]³⁺ complex (CA) can be successfully applied for the preparation of Au/SiO₂ catalysts with high metal loading, good dispersion, and small Au particle sizes.

Experimental Section

1. Au/SiO₂ Preparations. SiO₂ Degussa Aerosil 200 was used as support (BET surface area: 198 m² g⁻¹, average particle size of 12 nm, purity >99.5%). Absolute ethyl alcohol (Aldrich),

anhydrous diethyl ether (Sigma), ethylenediamine (Sigma), and crystalline H₂AuCl₄·3H₂O (Aldrich) as gold precursor were used for the preparation of [Au(en)₂]Cl₃. The [Au(en)₂]³⁺ complex was prepared as described by Block and Bailar.³³ Before cation adsorption of [Au(en)₂]³⁺, SiO₂ was dried in air at 100 °C for at least 24 h. All the preparations were performed in the absence of light, which is known to decompose the gold precursors.

For the preparation of Au/SiO₂ samples, 1 g of SiO₂ was dispersed in 100 mL of an aqueous solution of [Au(en)₂]Cl₃ (4 × 10⁻³ M) previously heated to 45 °C. The amount of gold in solution corresponds to a maximum gold loading of 7 wt % on SiO₂. To promote the cationic adsorption of [Au(en)₂]³⁺ complex on SiO₂, the solution pH was adjusted to the values higher than IEP_{SiO₂} by dropwise addition of 0.1 or 1 M ethanediamine solution. The suspension was vigorously stirred for 1 to 16 h at 45 °C in a thermostated vessel.

After the deposition of gold onto SiO₂, all the samples were submitted to the following procedure: solid separation—the suspended solids were separated from the precursor solution by centrifugation (5000 rpm for 10 min); washing—the separated solids were resuspended in water (100 mL g⁻¹), stirred for 10 min at 40 °C, and centrifuged again with this washing procedure being repeated four times to remove residual Cl⁻ ions as well as Au species not interacting with the support; drying—the washed solids were dried under vacuum at 25 °C for 12 h; thermal treatment—100 mg of sample were heated in a flow (100 mL min⁻¹) of industrial-grade air or ultrapure hydrogen (both from Praxair) from room temperature to the final temperature at a heating rate of 2 °C min⁻¹, followed by a 4-h isothermal step at the final temperature (this thermal treatment leads to the decomposition of Au(III) complexes into gold metal particles; it must be remembered that the thermal treatment used to reduce Au^{III} into Au⁰ can be performed with any gas (reducing gases such as H₂, or oxidizing gases such as air); when the supported gold precursor thermally decomposes in air, it forms Au⁰ because of the instability of Au^{III} species ($\Delta H_f(\text{Au}_2\text{O}_3) = 19.3 \text{ kJ mol}^{-1}$)³⁷); storage—all the samples were kept away from light and under vacuum in a desiccator at room temperature (a careful storage of the samples under the conditions specified is crucial; in fact, a strong increase in the average particle size in the calcined samples was observed when the samples were exposed to air even for a short period³⁸).

Guillemot with co-workers^{35,39} showed in a work on the preparation of gold catalysts supported on Y zeolite that the [Au(en)₂]³⁺ complex tends to decompose when it is heated to temperatures above 60–70 °C. As a consequence, they suggested that gold is reduced by ethanediamine ligands so that the preparation has to be performed at temperatures below 60 °C to avoid the complex decomposition and the reduction of gold. Indeed, the XANES study of Au/TiO₂ prepared by cationic adsorption of [Au(en)₂]³⁺ performed by one of us²⁵ revealed the presence of metallic gold in the sample prepared at 80 °C. The low stability of [Au(en)₂]³⁺ complex is certainly due to the metallic gold, which originated from the decomposition of [Au(en)₂]³⁺ in solution during the adsorption and subsequent deposition of metal gold colloids. In the same work, it was shown that the samples prepared at 25 °C do not contain metallic gold, but at the same time the maximum gold loading is low (~1 wt %). Therefore, in this work we decided to work at 45 °C, to avoid the decomposition of [Au(en)₂]³⁺ and to favor the cationic adsorption.

2. Characterization Techniques. Thermally treated Au/SiO₂ samples were examined by transmission electron microscopy (TEM) with a 2010 FasTem analytical microscope equipped

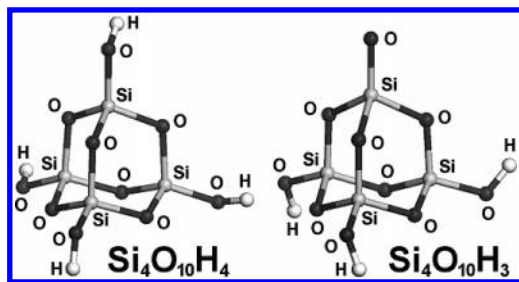


Figure 1. Optimized geometries of the neutral cluster Si₄O₁₀H₄ and the negatively charged cluster Si₄O₁₀H₃ used to model neutral and negatively charged silica surfaces, respectively.

with a Z-contrast annular detector. The histograms of the metal particle sizes were established from the measurement of 500 to 1000 particles. The size limit for the detection of gold particles on SiO₂ was about 1 nm. The average particle diameter \bar{d} was calculated from the following formula: $\bar{d} = \sum n_i d_i / \sum n_i$, where n_i is the number of particles of diameter d_i . The standard deviation was calculated from the following formula: $\sigma = [(\sum (d_i - \bar{d})^2) / \sum n_i]^{1/2}$.

Chemical analysis of Au in the samples was performed by energy-dispersive X-ray spectroscopy (EDS) with a detector Oxford-ISIS coupled to a scanning electron microscope (JEOL JSM-5900-LV). Chemical analyses were performed after thermal treatment of the samples. The Au weight loading is expressed in grams of Au per gram of sample wt % Au = $[m_{Au} / (m_{Au} + m_{SiO_2})] \times 100$.

Diffuse reflectance UV–visible spectra were obtained by using an Ocean Optics USB2000 miniature fiber optic spectrometer. Thermal analyses were carried out on a Jupiter Netzsch simultaneous TGA-DSC analyzer, under air (50 mL/min) at a heating rate of 10 °C min⁻¹. The Raman spectra were obtained with a Nicolet Almega micro-Raman dispersive equipment, using an excitation source of 532 nm.

3. Theoretical Calculations. The electronic structure calculations were performed with DMol³ numerically based density-functional theory (DFT) computer software implemented in Materials Studio Modeling 3.2 package from Accelrys Inc. We employed the Perdew–Wang PW91 general gradient approximation (GGA) in conjunction with double numerical basis set DND having a polarization d-function on all non-hydrogen atoms. Due to the presence of gold atoms in the model systems, DFT semilocal pseudopotentials were used instead of all-electron core treatment. Apparently for the same reason, the default convergence settings did not work well for geometry optimization, and convergence problems were found; a way to override them was to increase the maximum number of iterations and SCF cycles to 1000. The global orbital cutoff was 4.000 Å.

Neutral and negatively charged silica surfaces were simulated by neutral cluster Si₄O₁₀H₄ and negatively charged cluster Si₄O₁₀H₃, respectively (Figure 1).

Results and Discussion

Table 1 shows the gold loading and average particle size of Au/SiO₂ samples prepared by cationic adsorption. All the samples presented in Table 1 were reduced in H₂ at 200 °C. The natural pH of the original [Au(en)₂]Cl₃ solution with SiO₂ in suspension is 3.8, and under these conditions (CA1 sample) the Au loading is low (0.2 wt %) and the gold particle size is 1.5 nm. When the pH was increased (7, 9, and 10.5) the Au loading in Au/SiO₂ samples also increased in a proportional way. For the samples prepared at pH 7 (CA2), 9 (CA3), and 10.5 (CA4) the gold loading was 2.1, 3.3, and 5.5 wt %, respectively.

TABLE 1: Au/SiO₂ Samples Prepared by Cationic Adsorption of [Au(en)₂]³⁺ at 45 °C and Reduced in H₂ at 200 °C

sample	preparation		results		
	time of contact (h)	pH	Au loading (wt %)	av particle size (nm)	standard deviation (nm)
CA1	2	3.8 ^a	0.2	1.5	0.42
CA2	2	7	2.1	1.5	0.51
CA3	2	9	3.3	1.8	0.44
CA4	2	10.5	5.5	2.4	0.52
CA5	4	9	3.8	2.5	0.48
CA6	16	9	4.0	2.9	0.82

^a Natural pH.

respectively. Therefore, the increase of pH (from 3.8 to 10.5) leads to a significant increase in the Au loading (from 0.2 to 5.5 wt %). On the other hand, the gold particle size (1.5 nm) did not increase when pH was changed from 3.8 to 7, and slightly increased at pH 9 and 10.5 (to 1.8 and 2.4 nm, respectively).

Another parameter studied was the adsorption time, varied from 2 to 16 h (samples CA3, CA5, and CA6). The gold loading slightly increased from 3.3 to 4.0 wt %, while the average particle size increased from 1.8 to 2.9 nm (Table 1). The particle size distribution became broader when the adsorption time increased (Table 1).

In all cases, the TEM images showed highly dispersed gold nanoparticles on the surface of SiO₂ as is exemplified in Figure 2a. Conventional HRTEM images are shown in Figure 2b. The images were obtained at the optimum defocus condition to observe Au nanoparticles. Different morphologies are present as a function of the particle size. The particles with a size of 3 to 5 nm show defective structure, some of them exhibiting a multiple twinning particle (MTP) pattern, whereas the nanoparticles with an average size of ca. 2 nm have a defect-free structure with readily visible {111} family planes (Figure 2c,d). Additional information on the spatial distribution of Au nanoparticles over SiO₂ was obtained from the Z-contrast imaging of Au/SiO₂ (Figure 3). The High Angle Annular Dark Field technique (HAADF) can provide highly detailed images of nanocrystal surfaces, 3D information, and mass contrast simultaneously. The contrast in this type of images depends basically on the atomic number (Z); in Figure 3, the brighter zones correspond to Au nanoparticles. Figure 3a demonstrates the surface distribution of Au nanoparticles, where the differences in contrast indicate that gold is not agglomerated. Gold is present on the surface of SiO₂ only as small particles, which is evident from Figure 3a,b, where the Z contrast technique generates images with the high angle scattered electrons.

In all the tested experimental conditions, the solution pH (from 3.8 to 10.5) was higher than IEP_{SiO₂} (~2),³¹ so that the adsorption of [Au(en)₂]³⁺ was always possible. However, as was mentioned above, the gold loading is very dependent on the solution pH. This can be explained by the increase in the amount of negatively charged species present on the SiO₂ surface. The more the solution pH is above the pH of IEP, the more sites at the SiO₂ surface become negatively charged, and correspondingly the higher number of [Au(en)₂]³⁺ species is adsorbed. This indicates that the deposition of gold probably takes place according to a cationic adsorption mechanism, which leads to a high dispersion of the gold precursors and to small metal particle sizes after thermal treatment.

To give an insight into the adsorption mechanisms of [Au(en)₂]³⁺ ions on the SiO₂ surface, we performed a series of geometry optimizations using the PW91 GGA method in

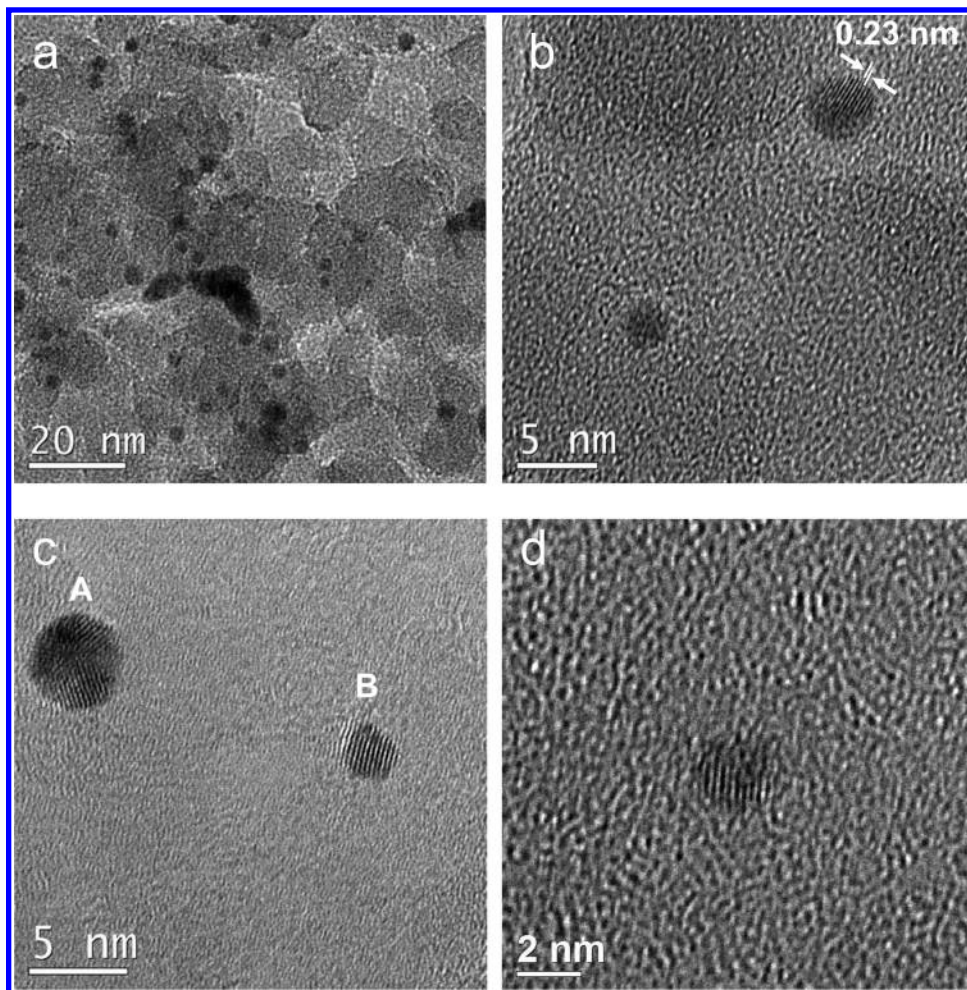


Figure 2. (a) Low-magnification TEM micrograph showing the particle distribution on the SiO₂ surface. (b) HRTEM image of gold nanoparticles. (c) HRTEM image of gold nanoparticles with different morphologies (A corresponds to a MTP and B corresponds to a FCC nanoparticle). (d) Gold nanoparticle of 2-nm size exhibiting the {111} family planes.

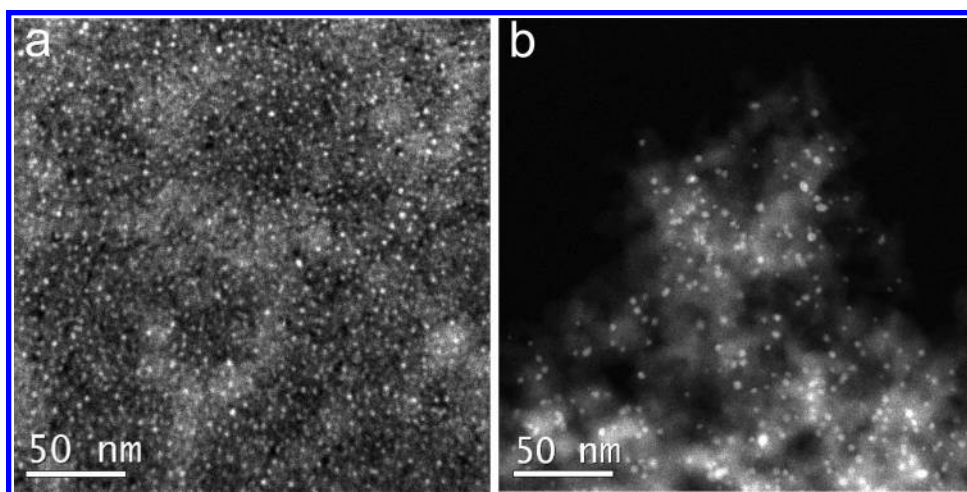


Figure 3. (a) HAADF image showing surface distribution of the gold nanoparticles. (b) A higher magnification image where it is possible to observe the contrast differences between the matrix and the nanoparticles. No gold agglomerates are present.

conjunction with the DND basis set. As shown in Figure 4a, all the Au–N coordination bonds in free [Au(en)₂]³⁺ ion are almost equal (2.114–2.116 Å). Both *trans*-N–Au–N angles are 180°, so that the coordination sphere is planar. These parameters notably change in the adsorption complexes [Au(en)₂Si₄O₁₀H₄]³⁺ and [Au(en)₂Si₄O₁₀H₃]²⁺. In the former case, which models [Au(en)₂]³⁺ adsorption on a neutral silica surface, the length of Au–N bonds remains relatively uniform,

of 2.076 to 2.116 Å (Figure 4b). At the same time, the coordination sphere undergoes considerable distortion, where *trans*-N–Au–N angles reduce to 174.3° and 178.5°. This distortion becomes even more manifested in the complex [Au(en)₂Si₄O₁₀H₃]²⁺, which corresponds to [Au(en)₂]³⁺ adsorption on a negatively charged silica surface. The *trans*-N–Au–N angles further reduce to 173.1° and 178.0°, and Au–N bond lengths vary from 2.028 to 2.184 Å (Figure 4c). Here one should

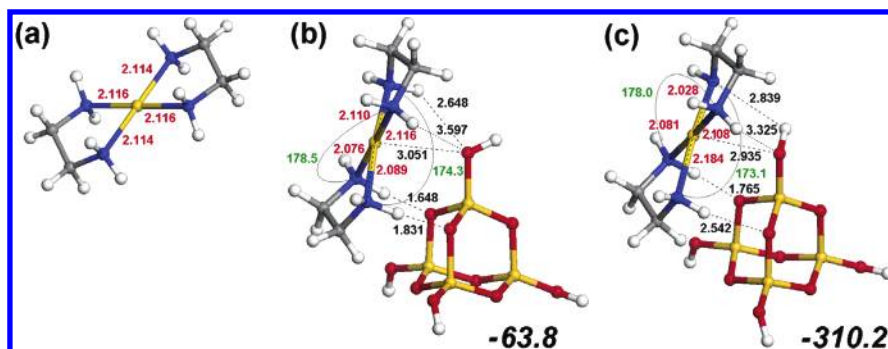


Figure 4. Optimized geometries for the gold complexes (a) $[\text{Au}(\text{en})_2]^{3+}$, (b) $[\text{Au}(\text{en})_2\text{Si}_4\text{O}_{10}\text{H}_4]^{3+}$, and (c) $[\text{Au}(\text{en})_2\text{Si}_4\text{O}_{10}\text{H}_3]^{2+}$. The values specified are formation energies of the adsorption complexes (in kcal mol^{-1}) (italics), *trans*-N–Au–N angles in degrees (green), Au–N bond distances (red) and some other selected interatomic distances (black) in angstroms. Element colors: C, gray; H, white; N, blue; O, red; and Au and Si, yellow.

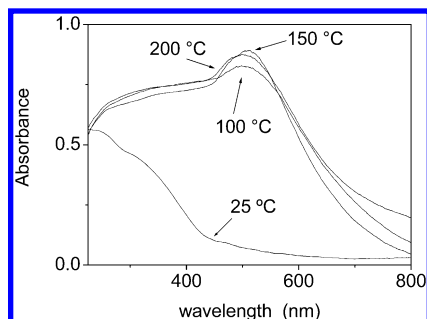


Figure 5. Diffuse reflectance UV–visible spectra of sample CA4 as a function of the temperatures of drying (25 °C) and reduction under hydrogen (100, 150, and 200 °C).

mention a somewhat unexpected result, namely, that upon geometry optimization, one hydrogen atom of the (upper rear) NH₂ group transferred completely to the initially deprotonated Si–O group of the Si₄O₁₀H₃ cluster. It is the deprotonated amino group that forms the shortest Au–N bond of 2.028 Å. In none of the model surface complexes have we found direct interaction of the Au atom with the cluster; the closest approach was the one to the oxygen atom of the Si–O–H group, which remained as long as 3.051 Å in $[\text{Au}(\text{en})_2\text{Si}_4\text{O}_{10}\text{H}_4]^{3+}$ and 2.935 Å in $[\text{Au}(\text{en})_2\text{Si}_4\text{O}_{10}\text{H}_3]^{2+}$. On the other hand, hydrogen bonding can be clearly observed between the N–H groups of the (left) ethylenediamine ligand and siloxane bridges of the silica clusters. In $[\text{Au}(\text{en})_2\text{Si}_4\text{O}_{10}\text{H}_4]^{3+}$, this bonding involves two N–H groups, with the NH \cdots O distances of 1.648 and 1.831 Å. In $[\text{Au}(\text{en})_2\text{Si}_4\text{O}_{10}\text{H}_3]^{2+}$, only one NH \cdots O separation (1.765 Å) can be qualified as an H-bond, whereas the second one increases to 2.542 Å. The opposite ethylenediamine ligand remains separated from the Si–O–H group by more than 2.5 Å in both adsorption complexes. The calculated formation energies (Figure 4) exhibit even larger differences than the geometric parameters do. While the value of $-63.8 \text{ kcal mol}^{-1}$ was obtained for $[\text{Au}(\text{en})_2\text{Si}_4\text{O}_{10}\text{H}_4]^{3+}$, it is $-310.2 \text{ kcal mol}^{-1}$ for $[\text{Au}(\text{en})_2\text{Si}_4\text{O}_{10}\text{H}_3]^{2+}$. Thus, the theoretical calculations are totally consistent with our suggestion that the deposition of gold takes place according to a cationic adsorption mechanism.

Figure 5 shows the diffuse-reflectance UV–visible spectra between 200 and 800 nm of the CA4 sample dried under vacuum at room temperature, and thermally treated in hydrogen at 100, 150, and 200 °C. The spectrum of the sample dried at room temperature under vacuum only presents an increasing reflectance signal starting at about 400 nm. The spectra of the samples treated in hydrogen exhibit a band around 550 nm, the intensity of which increases with the treatment temperature. This band is characteristic of the plasmon resonance of metallic gold particles. Such a resonance appears when the wavelength of

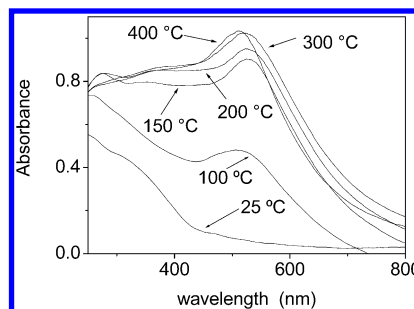


Figure 6. Diffuse reflectance UV–visible spectra of the CA4 sample as a function of the temperatures of drying (25 °C) and calcination under air (100, 150, 200, 300, and 400 °C).

the incident light far exceeds the particle diameter. The plasmon band is clearly visible after the treatment in hydrogen at 100 °C (Figure 5) and does not change at higher temperature (150 and 200 °C), suggesting that most of the gold is in the form of metallic particles at 100 °C.

On the other hand, Figure 6 presents the diffuse-reflectance UV–visible spectra of the same sample (CA4), dried under vacuum at room temperature and calcined in air at 100, 150, 200, 300, and 400 °C. The evolution of the plasmon band with temperature is different from that observed for the same samples treated in hydrogen. A weak plasmon band at $\sim 550 \text{ nm}$ is visible in the spectrum of the sample treated at 100 °C, which further increases after calcination at 150 °C. This confirms that metallic gold is present in the sample even when it is treated in air. The plasmon band intensity first increases with an increase in the treatment temperature, and then remains constant between 300 and 400 °C. It is known that the gold precursor decomposes in air with temperature to form Au⁰ due to the instability of Au^{III} species. Guillemot et al.³⁵ also suggested that Au³⁺ cations can be reduced by ethylenediamine ligands. As should be expected, gold is more easily reduced in hydrogen than in air. Furthermore, the spectra of the samples treated in air at 100, 150, and 200 °C exhibit an additional band in the region of 245–290 nm with a maximum at $\sim 275 \text{ nm}$, which is not observed for the samples treated in hydrogen, even at the lowest temperature of reduction (100 °C). This band disappears after 300 °C. Even if the literature data regarding the UV–visible absorption bands of gold coincide only in one point (i.e., that the absorption in the range of 500–600 nm results from the plasmon resonance of metallic gold particles), the band with maxima in the region of 240–320 nm was attributed to charge-transfer transitions in Au(I), Au(III) species, and gold charged clusters Au_{*n*}^{δ+}.^{40–44} From these results it is assumed that for samples treated in air at low temperature ($\leq 200 \text{ °C}$), both metallic and oxidized gold species are present. It has been shown by CO adsorption followed by FTIR studies that positive gold clusters are present

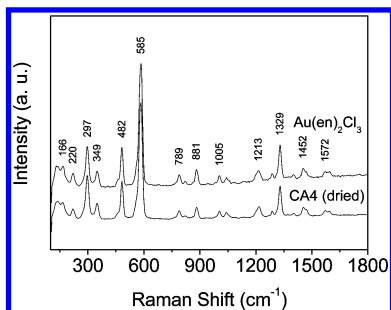


Figure 7. Raman spectra of the gold precursor $[\text{Au}(\text{en})_2]\text{Cl}_3$ and CA4 sample dried under vacuum at 25 °C.

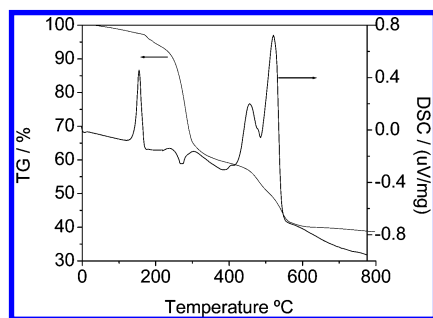


Figure 8. Thermogravimetric and differential scanning calorimetric analysis of $[\text{Au}(\text{en})_2]\text{Cl}_3$.

in Au/Y-zeolite samples prepared by cation exchange of $[\text{Au}(\text{en})_2]^{3+}$ after a calcination–reduction process.³⁴

The absence of the plasmon band in the sample dried at room temperature indicates that after preparation, and therefore during drying, gold is not reduced and probably remains in the oxidation state of the precursor, i.e., Au^{III} . Thus, the reduction of $[\text{Au}(\text{en})_2]^{3+}$ species on SiO_2 begins at low temperatures (<100 °C) even if the sample is treated in air.

Noteworthy is the change of color of the samples during preparation/treatment, which is also an indication of the oxidation state of gold. In the CA samples, the white color of the room temperature dried sample changed to dark red-brown after the reduction in hydrogen at 100 °C or higher temperatures. This dark red color is typical for metallic gold particles on SiO_2 .^{5,45,46} The Au/ SiO_2 samples also presented a reddish-brown color after calcinations (in air) at temperatures above 80 °C.

The $[\text{Au}(\text{en})_2]\text{Cl}_3$ and room temperature-dried Au/ SiO_2 samples were analyzed by Raman spectroscopy (Figure 7). Both spectra are remarkably coincident when they are superimposed, showing that the gold species deposited on SiO_2 during CA is precisely the $[\text{Au}(\text{en})_2]^{3+}$ complex. This result corroborates the fact that gold is not reduced during the CA process. A precise assignment of the vibrational modes of solid amine compounds is frequently complicated due to the band splitting.⁴⁷ Given this circumstance, the medium-intensity band at 1329 cm^{-1} as well as the weak and broad band at 1212 cm^{-1} can be attributed to the stretching $\nu(\text{C}-\text{N})$ vibrations, while the relatively weak bands between 1000 and 800 cm^{-1} are likely related to the NH_2 wagging/bending vibrations. Finally, the high-intensity band at 584 cm^{-1} together with those at 482, 348, and 297 cm^{-1} can be attributed to Au–N vibrations.⁴⁸

Figure 8 shows the thermogravimetric analysis (TGA) data of the complex $[\text{Au}(\text{en})_2]\text{Cl}_3$ treated in air at a heating rate of 10 °C/min. Initially, a mass loss of 5% (onset point 60 °C) along with a medium-intensity exothermic peak are observed, which may be due to the desorption/decomposition of residual chemical species coming from the synthesis of $[\text{Au}(\text{en})_2]\text{Cl}_3$ (ethanol was used for washing). After that, a continuous mass loss of 29%

(onset point 210 °C) associated with a low-intensity endothermic peak occurs, which can be related to the evolution of chlorides probably in the form of Cl_2 or even HCl (hydrogen atoms could be obtained from the amino groups). This assignment is consistent with the stoichiometric mass loss expected for the evolution of three chlorine atoms (plus eventually three more hydrogen atoms) in $[\text{Au}(\text{en})_2]\text{Cl}_3$, and with the occurrence of an endothermic peak. Finally, another complex mass loss of 25% (onset point 400 °C, end point 580 °C) takes place along with two exothermic peaks. Stoichiometrically this mass loss is consistent with the evolution of ethylenediamine species through a combustion process responsible for the exothermic peaks. At higher temperature, further changes are observed, and the residual mass (>40%) agrees with the expected one for metallic gold.

Conclusions

Liquid-phase methods such as deposition–precipitation, coprecipitation, and impregnation have not been effective to deposit small gold particles (<5 nm) onto SiO_2 . In this work we developed a new liquid-phase approach for the synthesis of small gold particles by the adsorption of $[\text{Au}(\text{en})_2]^{3+}$ cationic complex on an SiO_2 surface. We proposed and confirmed by theoretical calculations that the deposition of gold effectively takes place according to a cationic adsorption mechanism.

When the solution pH increases, the Au loading in Au/ SiO_2 samples increases in a proportional way and the average gold particle size slightly increases. This can be explained by the increase in the number of negatively charged species present on SiO_2 surface: when solution pH increases, a higher number of $[\text{Au}(\text{en})_2]^{3+}$ species can be adsorbed. Extending the adsorption time also produced a slight increase in gold loading. In all cases gold is not agglomerated on the SiO_2 support. The morphologies of gold nanoparticles were different depending on the particle size. The particles with an average size of 2 nm exhibit mainly fcc structures, whereas the particles of 3–5-nm size exhibit a multiple twinning particle structure.

To decompose the $[\text{Au}(\text{en})_2]^{3+}$ complex and generate gold nanoparticles, the dried samples were thermally treated in hydrogen or in air. According to UV–visible absorption measurements, a major fraction of gold is present in the form of metallic particles when samples were treated in hydrogen at 100 °C. For samples treated in air at low temperature (≤ 200 °C), both metallic and oxidized gold species are present. During the cationic complex adsorption and subsequent drying, gold is not reduced, and the gold species deposited on SiO_2 remain as the $[\text{Au}(\text{en})_2]^{3+}$ complex.

The results presented here suggest a new and simple liquid-phase method for the deposition of gold nanoparticles onto SiO_2 . As we showed previously, the cation adsorption can produce small gold particles on reducible supports such as TiO_2 . Now this preparation method will allow a more reliable comparison of catalytic activities of gold nanoparticles supported on reducible and inert supports, prepared through the same experimental approach. In addition these Au/ SiO_2 samples could be used in studies of linear and nonlinear optics. We also expect that the cation adsorption of $[\text{Au}(\text{en})_2]^{3+}$ can be used for the preparation of small gold particles on mesoporous materials such as MCMs y SBAs.

Acknowledgment. We are thankful to R. Sato for Raman spectra acquisition assistance and L. Rendon for HRTEM observation assistance. The authors are also thankful to the Central Microscopy facilities of the Institute of Physics, UNAM

for providing its microscope tools used in this work and the CUDI project for financial support of the HRTEM work. V.A.B. appreciates financial support from UNAM (grant DGAPA-IN100303).

References and Notes

- (1) Haruta, M.; Kageyama, H.; Kamijo, N.; Kobayashi, T.; Delannay, F. *Stud. Surf. Sci. Catal.* **1988**, *44*, 33.
- (2) Haruta, M.; Kobayashi, T.; Sano, H.; Yamada, N. *Chem. Lett.* **1987**, *2*, 405.
- (3) Haruta, M.; Yamada, N.; Kobayashi, T.; Iijima, S. *J. Catal.* **1989**, *115*, 301.
- (4) Haruta, M. *Catal. Today* **1997**, *36*, 153.
- (5) Bond, G. C.; Thompson, D. T. *Catal. Rev. Sci. Eng.* **1999**, *41*, 319.
- (6) Haruta, M. *Cattech* **2002**, *6*, 102.
- (7) Horvath, D.; Toth, L.; Guzzi, L. *Catal. Lett.* **2000**, *67*, 117.
- (8) Schubert, M. M.; Hackenberg, S.; Veen, A. C. v.; Muhler, M.; Plzak, V.; Behm, R. J. *J. Catal.* **2001**, *197*, 113.
- (9) Valden, M.; Pak, S.; Lai, X.; Goodman, D. W. *Catal. Lett.* **1998**, *56*, 7.
- (10) Zanella, R.; Giorgio, S.; Shin, C. H.; Henry, C. R.; Louis, C. *J. Catal.* **2004**, *222*, 357.
- (11) Zanella, R.; Louis, C.; Giorgio, S.; Touroude, R. *J. Catal.* **2004**, *223*, 328.
- (12) Valden, M.; Lai, X.; Goodman, D. W. *Science* **1998**, *281*, 1647.
- (13) Valden, M.; Goodman, W. *Isr. J. Chem.* **1998**, *38*, 285.
- (14) Boccuzzi, F.; Chiorino, A.; Manzoli, M.; Andreeva, D.; Tabakova, T. *J. Catal.* **1999**, *188*, 176.
- (15) Haruta, M.; Daté, M. *Appl. Catal. A* **2001**, *222*, 427.
- (16) Bond, G. C.; Thompson, D. T. *Gold Bull.* **2000**, *33*, 41.
- (17) Haruta, M.; Tsubota, S.; Kobayashi, T.; Kageyama, H.; Genet, M. J.; Delmon, B. *J. Catal.* **1993**, *144*, 175.
- (18) Bollinger, M. A.; Vannice, M. A. *Appl. Catal. B* **1996**, *8*, 417.
- (19) Tsubota, S.; Nakamura, T.; Tanaka, K.; Haruta, M. *Catal. Lett.* **1998**, *56*, 131.
- (20) Kozlov, A. I.; Kozlova, A. P.; Liu, H.; Iwasawa, Y. *Appl. Catal. A* **1999**, *182*, 9.
- (21) Liu, H.; Kozlov, A. I.; Kozlova, A. P.; Shido, T.; Iwasawa, Y. *Phys. Chem. Chem. Phys.* **1999**, *1*, 2851.
- (22) Guzzi, L.; Petö, G.; Beck, A.; Frey, K.; Geszti, O.; Molnár, G.; Daeóczy, C. *J. Am. Chem. Soc.* **2003**, *125*, 4332.
- (23) Petö, G.; Molnár, G. L.; Pászti, Z.; Geszti, O.; Beck, A.; Guzzi, L. *Mater. Sci. Eng., C* **2002**, *19*, 95.
- (24) Bar, T.; Visart-de-Bocarme, T.; Nieuwenhuys, B. E.; Kruse, N. *Catal. Lett.* **2001**, *74*, 127.
- (25) Zanella, R.; Delannoy, L.; Louis, C. *Appl. Catal. A* **2005**, *291*, 62.
- (26) Wolf, A.; Schüth, F. *Appl. Catal. A* **2002**, *226*, 1.
- (27) Lin, S. D.; Bollinger, M.; Vannice, M. A. *Catal. Lett.* **1993**, *17*, 245.
- (28) Resch, R.; Meltzer, S.; Vallant, T.; Hoffmann, H.; Koel, B. E.; Madhukar, A.; Requicha, A. S. G.; Will, P. *Langmuir* **2001**, *17*, 5666.
- (29) Okumura, M.; Nakamura, S.; Tsubota, S.; Nakamura, T.; Azuma, M.; Haruta, M. *Catal. Lett.* **1998**, *51*, 53.
- (30) Schimpf, S.; Lucas, M.; Mohr, C.; Rodemerck, U.; Brückner, A.; Radnik, J.; Hofmeister, H.; Claus, P. *Catal. Today* **2002**, *72*, 63.
- (31) Parks, G. A. *Chem. Rev.* **1965**, *65*, 177.
- (32) Iler, R. *The Chemistry of Silica*; John Wiley and Sons: New York, 1979.
- (33) Block, B. P.; Bailar, J. C., Jr. *J. Am. Chem. Soc.* **1951**, *73*, 4722.
- (34) Guillemot, D.; Borovskov, V. Y.; Kazansky, V. B.; Polisset-Thfoin, M.; Fraissard, J. *J. Chem. Soc., Faraday Trans.* **1997**, *93*, 3587.
- (35) Guillemot, D.; Polisset-Thfoin, M.; Fraissard, J. *Catal. Lett.* **1996**, *41*, 143.
- (36) Zanella, R.; Giorgio, S.; Henry, C. R.; Louis, C. *J. Phys. Chem. B* **2002**, *106*, 7634.
- (37) Bond, G. C. *Gold Bull.* **2001**, *34*, 117.
- (38) Zanella, R.; Louis, C. *Catal. Today* **2005**, *107–108*, 768.
- (39) Guillemot, D. Ph.D. Dissertation, Université Paris VI, 1997.
- (40) Salama, T.; Shido, T.; Ohnishi, R.; Ichikawa, M. *J. Phys. Chem.* **1996**, *100*, 3688.
- (41) Pestryakov, A.; Tuzovskaya, I.; Smolentseva, E.; Bogdanchikova, N.; Jentoft, F. C.; Knop-Gericke, A. *Int. J. Mod. Phys.* **2005**, *19*, 2321.
- (42) Pestryakov, A. N.; Lunin, V. V.; Kharlanov, A. N.; Kochubey, D. I.; Bogdanchikova, N.; Stakheev, A. Y. *J. Mol. Struct.* **2002**, *642*, 129.
- (43) Smolentseva, E.; Pestryakov, P.; Bogdanchikova, N.; Simakov, A.; Avalos, M.; Farias, M.; Diaz, J.; Gurin, V.; Tompos, A. *Int. J. Mod. Phys.* **2005**, *19*, 2496.
- (44) Chen, W.; Zhang, J.; Cai, W. *Scr. Mater.* **2003**, *48*, 1061.
- (45) Bond, G. C.; Sermon, P. A.; Webb, G.; Buchanan, D. A.; Wells, P. B. *Chem. Commun.* **1973**, 444.
- (46) Sermon, P. A.; Bond, G. C.; Wells, P. B. *J. Chem. Soc., Faraday Trans. 1* **1979**, *75*, 385.
- (47) Pouchert, C. J. *The Aldrich Library of Infrared Spectra*, 3rd ed.; Aldrich Chemical Co.: Milwaukee, WI, 1981.
- (48) Socrates, G. *Infrared Characteristic Group Frequencies, Tables and Charts*, 2nd ed.; Wiley: New York, 1994.